PROCEEDINGS OF SCIENCE

T-mu phase diagram using classical-quantum hybrid algorithm

Akio Tomiya[a,b,*]

[a] *International Professional University of Technology in Osaka*
Faculty of Technology and Science, International Professional University of Technology, 3-3-1, Umeda, Kita-ku, Osaka, 530-0001, Osaka, Japan

[b] *RIKEN/BNL Research center, Brookhaven National Laboratory, Upton, NY, 11973, USA*

E-mail: akio@yukawa.kyoto-u.ac.jp

We study the Schwinger model at finite temperature and density using a variational algorithm for near-term quantum devices. We adapt β-VQE, a classical-quantum hybrid algorithm with a neural network, to evaluate thermal and quantum expectation values and study the phase diagram for the massless Schwinger model along with the temperature and density. By comparing the exact variational free energy, we find that the variational algorithm works for the Schwinger model for $T > 0$ and μ>0. As a result, we obtain a qualitative picture of the phase diagram for the massless Schwinger model.

The 39th International Symposium on Lattice Field Theory,
8th-13th August, 2022,
Rheinische Friedrich-Wilhelms-Universität Bonn, Bonn, Germany

*Speaker

PoS(LATTICE2022)039

1. Introduction

QCD phase diagram is one of the most essential subjects in particle physics and nuclear physics [1–3] to understand the inside of nucleon stars and the history of the universe. At zero quark chemical potential, lattice QCD calculations with Markov chain Monte-Carlo (MCMC) work well and we can access quantitative information [4–9].

QCD phase structure along with finite baryon or quark density cannot be accessed using MCMC due to the infamous sign problem, and a number of proposals are suggested (see [3, 10–12] and references therein). For example, the complex Langevin algorithm has been applied not only to matrix models and toy models, but also to QCD in four dimensions [13–16]. The Lefschetz thimble algorithm is a similar approach, but it is an exact algorithm [17–20]. These methods are classified as classical algorithms, but there are also tensor network-based methods [21–27].

Algorithms for digital quantum computers for lattice QCD are highly demanded to overcome the sign problem [28, 29]. Quantum algorithms can be used to realize a unitary operation on the quantum state composed by elementary unitary operations on qubits. Quantum computations have been applied for the real-time (Lorentzian signature field theory) [30–32] and θ vacuum [33]. Standard classical algorithms are better at simulations with imaginary time, while systems with chemical potential and/or with the real-time axis are relatively straightforward for quantum algorithms. That is, quantum algorithms and classical algorithms have complementary advantages.

In this work, we study the phase diagram of the massless Schwinger model. We employ a classical-quantum hybrid algorithm called β-VQE [34] with the staggered fermion. This paper is organized as follows. First, we briefly review β-VQE and describe our theoretical setup. Second, we show our results with a quantum simulator on a classical machine. Finally, we summarize this work. As a result, we obtain phase diagram with temperature and chemical potential for the Schwinger model at the continuum limit.

2. Theoretical setup

2.1 β-VQE

Here we briefly review β-VQE [34]. The original variational quantum eigensolver (VQE) is a variational quantum for preparing the ground state [35], which is used in quantum chemistry and field theory. It uses a parametrized quantum circuit and minimizes the energy, namely the eigenvalue of the Hamiltonian for the target system. Thanks to the variational principle, if the eigenvalue is minimized, the state can be regarded as the (precisely approximated) ground state.

β-VQE [34] is an extension of VQE for mixed states, which typically appear when we treat thermal states[1]. The density matrix formalism is the best way to describe mixed states. Consider a pure state $|\Psi\rangle$, the density matrix is $\rho = |\Psi\rangle\langle\Psi|$. Mixed states can be written as $\rho_{\text{mixed}} = \sum_i w_i \rho_i$ where ρ_i is a density matrix for the pure state and w_i is a probability weight to find a state ρ_i. This is conceptually different from the superposition of states, which is a pure state.

In β-VQE, we minimize the following loss function,

$$\mathcal{L}(\Theta) = \mathrm{Tr}\left(\tilde{\rho}_\Theta \ln\left(\tilde{\rho}_\Theta/\rho\right)\right), \tag{1}$$

[1]Thermal states can be realized using pure states through [36–38]. In this work, we focus on mixed state realization.

where $\rho = \mathrm{e}^{-\frac{1}{T}H}/Z$ is the density matrix (normalized as $\mathrm{Tr}\,[\rho] = 1$) and H is the Hamiltonian of the target system with zero or nonzero chemical potential, and T is the temperature of the grand canonical ensemble. Θ represents a set of parameters. $\tilde{\rho}_\Theta$ is the parametrized density matrix (normalized as $\mathrm{Tr}\,[\tilde{\rho}_\Theta] = 1$). This loss function is the Kullback-Leibler-Umegaki (KLU) divergence, a quantum extension of the Kullback-Leibler divergence (equivalent to the relative entropy), and it takes zero if and only if $\tilde{\rho}_\Theta = \rho$. We minimize this loss function by tuning a set of parameters Θ. In practice, we minimize shifted KLU divergence $\mathcal{L}(\Theta) - \ln Z = \mathrm{Tr}(\tilde{\rho}_\Theta \ln \tilde{\rho}_\Theta) + \frac{1}{T}\mathrm{Tr}(\tilde{\rho}_\Theta H)$ to avoid the calculation of the free energy $\ln Z$. We note that we can evaluate the quality of the variational state by comparing $\mathcal{L}(\Theta)$ and $\ln Z$ in the case of classial simulation of the variational method. We remark that the use of shifted KLU divergence is analogous to the use of Kullback-Leibler divergence in the flow-based sampling algorithm, a machine learning-assisted configuration generation algorithm [39, 40].

We employ a product state of N qubits, $|x\rangle = |x_1\rangle_1 \otimes |x_2\rangle_2 \otimes \cdots \otimes |x_N\rangle_N$ and each $|x_i\rangle_i$ is the state of a qubit ($i = 1, \cdots, N$). x is a bit string $x = x_1 x_2 \cdots x_N$ where $x_i \in \{0, 1\}$. We use $|x\rangle$ for an initial state of the variational procedure. VQE type variational approaches use a parametrized state $U_\theta\,|x\rangle$, where θ is a set of parameters for a quantum state and U_θ a set of unitary operation like a set of rotation gates and Hadamard gates. In practice, we use SU(4) parametrization for U_θ as in the original work [34]. We parametrize the density matrix as,

$$\tilde{\rho}_\Theta = \sum_x p_\phi(x) U_\theta |x\rangle\langle x| U_\theta^\dagger, \tag{2}$$

where $\Theta = \theta^\cup \phi$ and p_ϕ is a parametrized classical probability distribution of x. The sum of x is taken over all possible combinations of x. This density matrix satisfies the normalization condition $\mathrm{Tr}\,[\tilde{\rho}_\Theta] = \sum_x p_\phi(x) = 1$. In the application, we employ the autoregressive model [41], which is a neural network. As a unit of the autoregressive model, we utilize an autoencoder, which has single hidden layer of 500 hidden neurons with rectified linear unit activation function. This is the same setup as the original work for β-VQE [34].

Since β-VQE can produce training samples by itself, we rely on the self-training paradigm for the training. Practically we minimize following loss function which is equivalent to (1),

$$\mathcal{L}(\Theta) = \mathbb{E}_{x\sim p_\phi(x)}[\ln p_\phi(x) + \langle x|U_\theta^\dagger H U_\theta|x\rangle]/T + \text{const.} \tag{3}$$

where $\mathbb{E}_{x\sim p_\phi(x)}[\cdot]$ means that an expectation value evaluating with sampling of x from $p_\phi(x)$.

Minimization of the loss function $\mathcal{L}(\Theta)$ is performed by a stochastic gradient optimizer (*e.g.*, ADAM [42]). In the optimization procedure, we have to evaluate two kinds of gradients. One is a derivative with respect to parameters in the quantum circuit,

$$\nabla_\theta \mathcal{L}(\Theta) = \mathbb{E}_{x\sim p_\phi(x)}[\nabla_\theta \langle x|U_\theta^\dagger H U_\theta|x\rangle]/T. \tag{4}$$

This derivative can be evaluated using the shift rule [43, 44].

The other is a derivative with respect to parameters in the classical distribution,

$$\nabla_\phi \mathcal{L}(\Theta) = \mathbb{E}_{x\sim p_\phi(x)}\left[(f(x) - b)\nabla_\phi \ln p_\phi(x)\right], \tag{5}$$

where $f(x) = \ln p_\phi(x) + \langle x|U_\theta^\dagger H U_\theta|x\rangle/T$ and $b = \mathbb{E}_{x\sim p_\phi}[f(x)]$.

After training, one can sample a batch of input states $|x\rangle$ and treat them as approximations of the eigenstates of the system. By using the states, we can calculate observables with T and μ.

2.2 Schwinger model in spin representation

We investigate the massless Schwinger model which is QED in 1+1 dimensional spacetime. The Lagrangian of the Schwinger model with $\theta = 0$ is given by

$$\mathcal{L} = -\frac{1}{4}F_{\mu\nu}F^{\mu\nu} + \mathrm{i}\overline{\psi}\gamma^{\mu}\left(\partial_{\mu} + \mathrm{i}gA_{\mu}\right)\psi - m\overline{\psi}\psi, \tag{6}$$

where g is the dimension-full coupling constant. Massless Schwinger model can be solved exactly, with and without temperature [45, 46]. We discretize the spatial direction and we adopt the staggered formalism for the fermion field *a la*, Kogut and Susskind. Throughout this paper, we focus on $m = 0$ but we keep m for a while for showing purpose.

The U(1) gauge field can be eliminated from the hamiltonian in 1+1 dimension with the open boundary condition [30], and the remnant of it is a non-local four-fermi interaction term. Furthermore, using Jordan-Wigner transformation, we obtain the quantum spin representation of the system [30, 33, 47]. The final expression of the Hamiltonian is

$$\hat{H} = H/g = \hat{H}_{ZZ} + \hat{H}_{\pm} + \hat{H}_{Z}. \tag{7}$$

where

$$\hat{H}_{ZZ} = \frac{g}{8w}\sum_{n=2}^{N_x-1}\sum_{1\le k<l\le n} Z_k Z_l, \quad \hat{H}_{\pm} = \frac{1}{2}\sum_{n=1}^{N_x-1}\frac{w}{g}\left[X_n X_{n+1} + Y_n Y_{n+1}\right], \tag{8}$$

$$\hat{H}_{Z} = \frac{1}{2}\sum_{n=1}^{N_x}\left(\frac{m}{g}(-1)^n + \frac{\mu}{g}\right)Z_n - \frac{g}{8w}\sum_{n=1}^{N_x-1}(n \bmod 2)\sum_{l=1}^{n} Z_l \tag{9}$$

and $\hat{}$ indicates a dimensionless quantity. $w = 1/(2a)$, and N_x are (inverse) lattice spacing and the dimensionless spatial extent of the staggered fermions, respectively. Z_n, X_n and Y_n are Pauli matrices acting on the n-th qubit. We introduced the chemical potential μ by replacing the mass term, which does not occur the sign problem in this formalism because this based on the operator formalism in Lorentzian signature spacetime. The exponent of Boltzmann weight is now $H/T = (g/T)\hat{H}$, and g/T is dimensionless inverse temperature.

3. Results

Here we explain our numerical setup and show our results. Detail lattice setup and technical details can be found in [47]. We perform calculations for $N_x = 4, 6, 8$ and 10 with various lattice cutoff, temperature, and chemical potential. However, results for $N_x \le 6$ are supposed to be affected by finite volume effects [33] and we only use $N_x = 10$ for final results. For $N_x \ge 12$, calculation time or memory size is beyond our numerical capacity of resources with [34, 48].

We tune parameters in β-VQE, and calculate spatial averaged chiral condensate as in [33]. Results are shown in Fig. 1. Top two panels are results for $\hat{T} = 1/0.1 = 10$ (high temperature) and bottom two ones are $\hat{T} = 1/20.0 = 0.05$ (low temperature). Left and right panels are for $\hat{\mu} = 0$ and $\hat{\mu} = 1.4$, respectively. Solid lines are trained loss function and dotted lines are exact free energy $-\ln Z$ calculated by the exact diagonalization for comparison. State preparation for low temperature is harder than high temperature as expected.

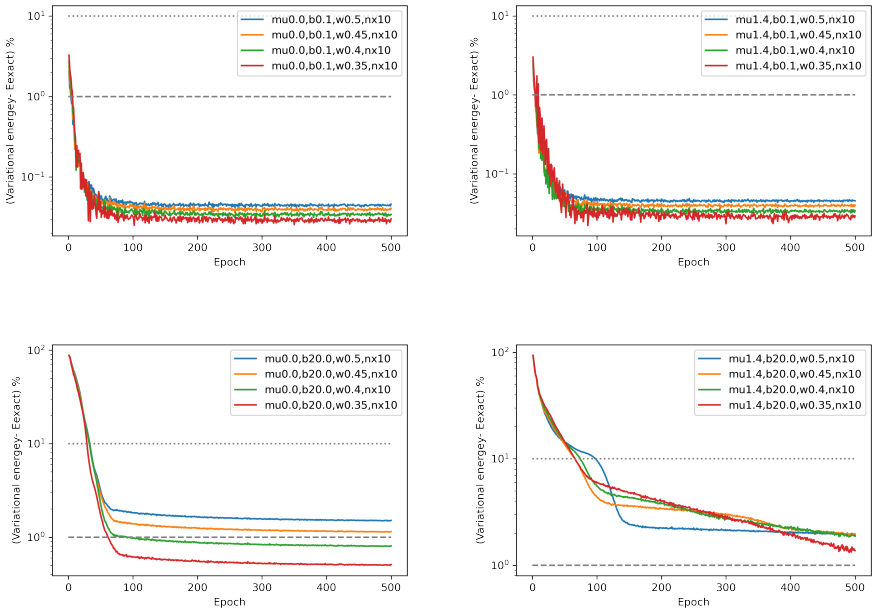

Figure 1: Training history of the loss function (Variational free energy) for various temperature, cutoff and chemical potential.

After β-VQE calculations, we take *naive* continuum limit of the chiral condensates[2] for $N_x = 8$ and $N_x = 10$. We confirm that, numerical results qualitatively follow the exact solution for $\mu = 0$. For $\mu > 0$, the chiral condensate is suppressed.

Finally, we make a density plot for $N_x = 10$ in the continuum limit (Fig 2). It has a non-trivial phase structure and to confirm this phase structure, we need data from larger lattice than $N_x = 10$.

4. Summary and conclusion

In this work, we investigate a phase diagram on finite temperature and density for the Schwinger model using a quantum classical hybrid algorithm called β-VQE, which is not affected by the sign problem. Quantum expectation values are evaluated through state vector calculations on a classical computer which should be replaced by quantum calculations in the future. Thanks to the state vector calculations, we evaluate the exact free energy $-\ln Z$ and we confirm that the variational algorithm gives $O(1)\%$ correct results.

Only continuum limit is taken and large volume limit has not been taken in this work. While, we observe qualitative agreement along with the temperature to the exact results for $\mu/g = 0$ [45] and the deviation is similar to [50]. To establish physics at infinity volume, we should replace the state-vector calculations to a tensor network or quantum device. We enphasize that β-VQE can

[2] In the conference, T. Angelides and E. Itou told me that a work [49] for chiral symmetry violation in the Schwinger model with the staggered fermion, but here we report original results as in the conference since results do not change qualitatively. This formalism has an additive mass renormalization.

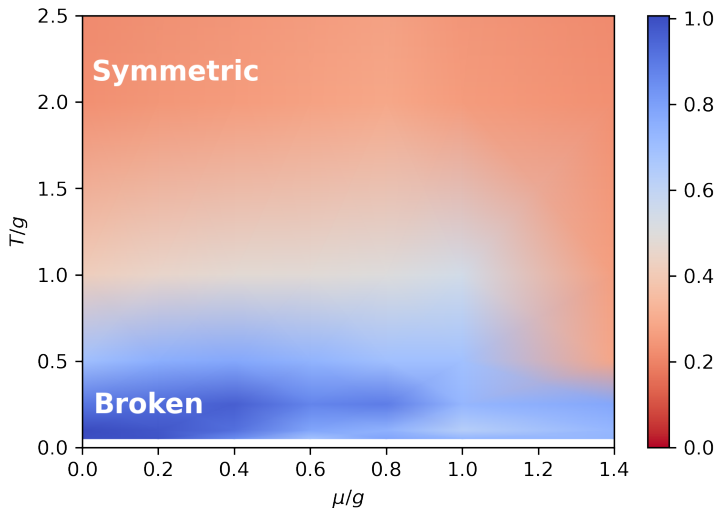

Figure 2: Density plot of the chiral condensate from β-VQE along with T/g and μ/g. The central values are interpolated. This density plot can be seen as the phase diagram.

be used with a quantum device, and once we get a fault-tolerant quantum computer, we can easily apply the calculations with it.

Acknowledgements

AT thanks Takis Angelides and Etuko Itou for letting him know an important reference for chiral symmetry violation for the staggered quark [49]. This work of AT was supported by JSPS KAKENHI Grant Number JP20K14479, JP22H05112, JP22H05111, and JP22K03539. Numerical computation in this work was partially carried out at the Yukawa Institute Computer Facility.

References

[1] N. Cabibbo and G. Parisi. Exponential hadronic spectrum and quark liberation. *Physics Letters B*, 59(1):67–69, 1975.

[2] Kenji Fukushima and Tetsuo Hatsuda. The phase diagram of dense QCD. *Rept. Prog. Phys.*, 74:014001, 2011.

[3] Jana N. Guenther. Overview of the QCD phase diagram: Recent progress from the lattice. *Eur. Phys. J. A*, 57(4):136, 2021.

[4] A. Bazavov et al. Fluctuations and Correlations of net baryon number, electric charge, and strangeness: A comparison of lattice QCD results with the hadron resonance gas model. *Phys. Rev. D*, 86:034509, 2012.

[5] Heng-Tong Ding, Frithjof Karsch, and Swagato Mukherjee. Thermodynamics of strong-interaction matter from Lattice QCD. *Int. J. Mod. Phys. E*, 24(10):1530007, 2015.

[6] A. Bazavov et al. Chiral crossover in QCD at zero and non-zero chemical potentials. *Phys. Lett. B*, 795:15–21, 2019.

[7] Szabolcs Borsanyi, Zoltan Fodor, Jana N. Guenther, Sandor K. Katz, Kalman K. Szabo, Attila Pasztor, Israel Portillo, and Claudia Ratti. Higher order fluctuations and correlations of conserved charges from lattice QCD. *JHEP*, 10:205, 2018.

[8] Frithjof Karsch. Critical behavior and net-charge fluctuations from lattice QCD. *PoS*, CORFU2018:163, 2019.

[9] Jishnu Goswami, Frithjof Karsch, Christian Schmidt, Swagato Mukherjee, and Peter Petreczky. Comparing conserved charge fluctuations from lattice QCD to HRG model calculations. *Acta Phys. Polon. Supp.*, 14:251, 2021.

[10] Christof Gattringer, Thomas Kloiber, and Vasily Sazonov. Solving the sign problems of the massless lattice Schwinger model with a dual formulation. *Nucl. Phys. B*, 897:732–748, 2015.

[11] Claudia Ratti. QCD at non-zero density and phenomenology. *PoS*, LATTICE2018:004, 2019.

[12] Andrei Alexandru, Gokce Basar, Paulo F. Bedaque, and Neill C. Warrington. Complex paths around the sign problem. *Rev. Mod. Phys.*, 94(1):015006, 2022.

[13] Gert Aarts, Erhard Seiler, Denes Sexty, and Ion-Olimpiu Stamatescu. Complex Langevin dynamics and zeroes of the fermion determinant. *JHEP*, 05:044, 2017. [Erratum: JHEP 01, 128 (2018)].

[14] Erhard Seiler. Status of Complex Langevin. *EPJ Web Conf.*, 175:01019, 2018.

[15] Casey E. Berger, Lukas Rammelmüller, Andrew C. Loheac, Florian Ehmann, Jens Braun, and Joaquín E. Drut. Complex Langevin and other approaches to the sign problem in quantum many-body physics. *Phys. Rept.*, 892:1–54, 2021.

[16] M. Scherzer, D. Sexty, and I. O. Stamatescu. Deconfinement transition line with the complex Langevin equation up to $\mu/T \sim 5$. *Phys. Rev. D*, 102(1):014515, 2020.

[17] Yuto Mori, Kouji Kashiwa, and Akira Ohnishi. Lefschetz thimbles in fermionic effective models with repulsive vector-field. *Phys. Lett. B*, 781:688–693, 2018.

[18] Christian Schmidt and Felix Ziesché. Simulating low dimensional QCD with Lefschetz thimbles. *PoS*, LATTICE2016:076, 2017.

[19] Genki Fujisawa, Jun Nishimura, Katsuta Sakai, and Atis Yosprakob. Backpropagating Hybrid Monte Carlo algorithm for fast Lefschetz thimble calculations. *JHEP*, 04:179, 2022.

[20] Masafumi Fukuma, Nobuyuki Matsumoto, and Yusuke Namekawa. Numerical sign problem and the tempered lefschetz thimble method. In *21st Hellenic School and Workshops on Elementary Particle Physics and Gravity*, 5 2022.

[21] M. C. Bañuls, K. Cichy, K. Jansen, and J. I. Cirac. The mass spectrum of the Schwinger model with Matrix Product States. *JHEP*, 11:158, 2013.

[22] Kai Zapp and Roman Orus. Tensor network simulation of QED on infinite lattices: Learning from (1+1) d , and prospects for (2+1) d. *Phys. Rev. D*, 95(11):114508, 2017.

[23] Lena Funcke, Karl Jansen, and Stefan Kühn. Topological vacuum structure of the Schwinger model with matrix product states. *Phys. Rev. D*, 101(5):054507, 2020.

[24] Nouman Butt, Simon Catterall, Yannick Meurice, Ryo Sakai, and Judah Unmuth-Yockey. Tensor network formulation of the massless schwinger model with staggered fermions. *Phys. Rev. D*, 101(9):094509, 2020.

[25] Masazumi Honda, Etsuko Itou, and Yuya Tanizaki. DMRG study of the higher-charge Schwinger model and its 't Hooft anomaly. *JHEP*, 11:141, 2022.

[26] Takuya Okuda. Schwinger model on an interval: analytic results and DMRG. 10 2022.

[27] Takis Angelides, Lena Funcke, Karl Jansen, and Stefan Kühn. Mass Renormalization of the Schwinger Model with Wilson and Staggered Fermions in the Hamiltonian Lattice Formulation. In *39th International Symposium on Lattice Field Theory*, 11 2022.

[28] Scott Lawrence. *Sign Problems in Quantum Field Theory: Classical and Quantum Approaches*. PhD thesis, Maryland U., 2020.

[29] Alexander M. Czajka, Zhong-Bo Kang, Henry Ma, and Fanyi Zhao. Quantum simulation of chiral phase transitions. *JHEP*, 08:209, 2022.

[30] E. A. Martinez et al. Real-time dynamics of lattice gauge theories with a few-qubit quantum computer. *Nature*, 534:516–519, 2016.

[31] Emilie Huffman, Miguel García Vera, and Debasish Banerjee. Real-time dynamics of Plaquette Models using NISQ Hardware. 9 2021.

[32] Wibe A. de Jong, Kyle Lee, James Mulligan, Mateusz Płoskoń, Felix Ringer, and Xiaojun Yao. Quantum simulation of non-equilibrium dynamics and thermalization in the Schwinger model. 6 2021.

[33] Bipasha Chakraborty, Masazumi Honda, Taku Izubuchi, Yuta Kikuchi, and Akio Tomiya. Classically emulated digital quantum simulation of the Schwinger model with a topological term via adiabatic state preparation. *Phys. Rev. D*, 105(9):094503, 2022.

[34] Jin-Guo Liu, Liang Mao, Pan Zhang, and Lei Wang. Solving quantum statistical mechanics with variational autoregressive networks and quantum circuits. *Machine Learning: Science and Technology*, 2(2):025011, 2021.

[35] Jules Tilly et al. The Variational Quantum Eigensolver: A review of methods and best practices. *Phys. Rept.*, 986:1–128, 2022.

[36] Sho Sugiura and Akira Shimizu. Thermal Pure Quantum States at Finite Temperature. *Phys. Rev. Lett.*, 108:240401, 2012.

[37] A. Tomiya. Tpq, 2020. https://conference-indico.kek.jp/event/113/contributions/2175/.

[38] Zohreh Davoudi, Niklas Mueller, and Connor Powers. Toward Quantum Computing Phase Diagrams of Gauge Theories with Thermal Pure Quantum States. 8 2022.

[39] M. S. Albergo, G. Kanwar, and P. E. Shanahan. Flow-based generative models for Markov chain Monte Carlo in lattice field theory. *Phys. Rev. D*, 100(3):034515, 2019.

[40] Akio Tomiya and Satoshi Terasaki. GomalizingFlow.jl: A Julia package for Flow-based sampling algorithm for lattice field theory. 8 2022.

[41] Mathieu Germain, Karol Gregor, Iain Murray, and Hugo Larochelle. MADE: masked autoencoder for distribution estimation. *CoRR*, abs/1502.03509, 2015.

[42] Diederik P. Kingma and Jimmy Ba. Adam: A method for stochastic optimization, 2014.

[43] Gavin E Crooks. Gradients of parameterized quantum gates using the parameter-shift rule and gate decomposition, 2019.

[44] Leonardo Banchi and Gavin E. Crooks. Measuring analytic gradients of general quantum evolution with the stochastic parameter shift rule. *Quantum*, 5:386, jan 2021.

[45] Ivo Sachs and Andreas Wipf. Finite temperature Schwinger model. *Helv. Phys. Acta*, 65:652–678, 1992.

[46] Y. Hosotani. Chiral dynamics in weak, intermediate, and strong coupling QED in two-dimensions. In *International Workshop on Perspectives of Strong Coupling Gauge Theories (SCGT 96)*, pages 390–397, 3 1997.

[47] Akio Tomiya. Schwinger model at finite temperature and density with beta VQE. *arXiv:2205.08860*, 5 2022.

[48] Xiu-Zhe Luo, Jin-Guo Liu, Pan Zhang, and Lei Wang. Yao.jl: Extensible, Efficient Framework for Quantum Algorithm Design. *Quantum*, 4:341, October 2020.

[49] Ross Dempsey, Igor R. Klebanov, Silviu S. Pufu, and Bernardo Zan. Discrete chiral symmetry and mass shift in the lattice hamiltonian approach to the schwinger model. *Phys. Rev. Res.*, 4:043133, Nov 2022.

[50] Mari Carmen Bañuls, Krzysztof Cichy, Karl Jansen, and Hana Saito. Chiral condensate in the Schwinger model with Matrix Product Operators. *Phys. Rev. D*, 93(9):094512, 2016.